Jurnal Teknik Sipil & Perencanaan vol (1) (2026) p 27-38

UNNES JOURNALS

JURNAL TEKNIK SIPIL & PERENCANAAN

https://doi.org/10.15294/jtsp.v28i1.48032

Probabilistic Seismic Hazard Analysis (PSHA) of Bali Airport Considering Earthquake Effects

Fazli Elahi [1, a)], Hanindya Kusuma Artati[2, b)], Achmed Pusha Agung [3, c)], Vinda Nurul Hidayatul Aiman [3, d)], Mohammad Subhan Rehman [3, e)], Irfan Ullah [3, f)]

[1]*Islam Indonesia University*
[2]*Islam Indonesia University*
[3]*Islam Indonesia University*

[a)]Corresponding author: 24914001@students.uii.ac.id
[b)]hanindya@uii.ac.id, [c)]24914002@students.uii.ac.id, [d)]24914014@students.uii.ac.id,
[e)]subhankhattak33@gmail.com, [e)]irfandawar11@gmail.com

Abstract. I Gusti Ngurah Rai International Airport in Bali is a critical national infrastructure located in a region of high seismicity driven by the Indo-Australian–Eurasian plate convergence. Despite the availability of national-level hazard maps, no site-specific probabilistic seismic hazard study incorporating local soil amplification has previously been conducted for this facility. This study performs site-specific Probabilistic Seismic Hazard Analysis (PSHA) using EZ-FRISK, one-dimensional non-linear soil amplification analysis using DEEPSOIL V7, and spectral matching of ground motions from the PEER NGA database to represent Bali seismic conditions. Historical earthquake data (Mw 4.0–9.0, 1900–2025) within a 500 km radius were compiled from the USGS catalog. Earthquake recurrence was characterized using the Gutenberg-Richter relationship. The Atkinson and Boore (2003) GMPE was applied for subduction sources. Bedrock PGA was determined at a 2% probability of exceedance in 50 years (return period = 2,475 years). Site response analysis was performed using N-SPT-derived shear-wave velocity profiles. Bedrock PGA is 0.308 g (design value 0.206 g after 2/3 factor). After nonlinear soil amplification, the surface PGA reaches 0.800 g, a 2.6-fold amplification, indicating a severe surface hazard. Hazard deaggregation identifies a dominant scenario earthquake of Mw 5.95 at 23.86 km. This is the first integrated PSHA study combining bedrock hazard, soil amplification, and spectral matching for Bali Airport, providing site-specific ground-motion parameters critical for earthquake-resistant structural design and liquefaction risk assessment at this strategically vital facility.

Keywords: probabilistic seismic hazard analysis (PSHA), peak ground acceleration (PGA), soil amplification, liquefaction, bali airport, DEEPSOIL, spectral matching

INTRODUCTION

Indonesia is one of the most seismically active countries in the world, situated at the convergence of the Indo-Australian, Eurasian, and Pacific plates [1]. The Java–Bali subduction zone, where the Indo-Australian Plate subducts beneath the Eurasian Plate at approximately 67 mm/year [2], generates recurring megathrust events, shallow crustal faults, and intermediate-depth intraslab earthquakes. Bali, located directly above this tectonic boundary, faces a compound seismic hazard from multiple source mechanisms. Recent destructive events, including the 2018 Lombok earthquakes (Mw 6.9) and the 2022 Cianjur earthquake (Mw 5.6), have reinforced the urgency of site-specific hazard assessment throughout this arc.

I Gusti Ngurah Rai International Airport (hereinafter "Bali Airport") is among Indonesia's busiest international gateways, handling over 23 million passengers annually before the COVID-19 pandemic [3]. Critical airport infrastructure, including runways, control towers, passenger terminals, and fuel facilities, must remain operational in the immediate aftermath of a major earthquake. Despite its strategic importance, no comprehensive site-specific PSHA incorporating local soil amplification has been published for this facility.

Although national-level probabilistic seismic hazard maps (PuSGeN 2017 [4]; SNI 1726:2019 [5]) provide zone-averaged design spectra, they do not capture site-specific ground motion amplification arising from local soil stratigraphy. Previous regional PSHA studies in Indonesia have focused on Semarang and Solo [6], Lombok [7], and West Sulawesi [8]. Still, none have addressed Bali Airport with integrated bedrock hazard analysis, site response, and spectral matching. The present study fills this gap by providing a comprehensive site-specific ground-motion characterization needed for performance-based earthquake engineering design at this critical facility.

The specific objectives of this study are:

- To quantify bedrock Peak Ground Acceleration (PGA) and Uniform Hazard Spectra (UHS) at Bali Airport for a 2% probability of exceedance in 50 years (return period 2,475 years) using PSHA.
- To perform hazard deaggregation to identify the dominant earthquake scenario (magnitude M and distance R) controlling the site hazard.
- To evaluate local soil amplification by propagating selected ground motions from bedrock to the surface using one-dimensional non-linear site response analysis (DEEPSOIL V7).
- To assess liquefaction potential at the airport site based on the amplified surface ground motions and N-SPT soil data.

Probabilistic Seismic Hazard Analysis (PSHA) was formalized by Cornell (1968) [9] and further developed by McGuire (1976, 2004) [10,11]. PSHA integrates earthquake source characterization, recurrence statistics, and ground-motion prediction to compute the annual rate of exceedance for ground-motion intensity measures such as PGA and spectral acceleration Sa(T). The Gutenberg-Richter (G-R) recurrence law [12] describes the frequency-magnitude relationship as $\log N = a - bM$, where a and b are region-specific constants derived from historical seismicity catalogs.

Ground Motion Prediction Equations (GMPEs) translate rupture parameters (magnitude, source-to-site distance, focal mechanism, site classification) into expected ground motion with associated aleatory variability. For subduction-zone environments analogous to the Java–Bali arc, the GMPE of Atkinson and Boore (2003) [13] developed for interface and intraslab events along the Cascadia and other subduction zones has been widely validated and adopted in Southeast Asian PSHA studies [6,7]. More recent GMPEs, such as those by BC Hydro (Abrahamson et al., 2016) [14] and Zhao et al. (2006) [15], have also been applied in Indonesian settings; their suitability relative to Atkinson and Boore (2003) was considered in the GMPE selection for this study.

Site response analysis accounts for the amplification or de-amplification of bedrock motion as seismic waves travel through soil layers. One-dimensional non-linear analysis using equivalent-linear or fully non-linear approaches (e.g., DEEPSOIL; Hashash et al. 2020 [16]) is the standard method for computing surface ground motion from bedrock input. The ratio of surface-to-bedrock spectral amplitude defines the site amplification factor, which is critical for accurate seismic design of structures on soft or medium-stiff soils, as commonly encountered in coastal Bali [17].

National seismic design in Indonesia is governed by SNI 1726:2019 [5], which prescribes design spectral accelerations (SDS, SD1) derived from PSHA-based probabilistic maps at a 2%/50-year hazard level. Site-specific procedures under this code allow engineers to substitute site-specific UHS for the default mapped values, provided a complete PSHA and site response study is conducted within the scope of the present work.

Table 1 summarises key previous PSHA and site-specific seismic hazard studies in Indonesia and comparable subduction environments, highlighting how the present study advances the state of knowledge.

Table 1. Summary of relevant previous PSHA studies and positioning of the present work

Asrurifak et al. (2010). [1]	National Indonesia	PSHA national scale	UHS for a 2,500-year return period	Zone-averaged; no site-specific amplification

Makrup & Muntafi (2016). [6]	Semarang & Solo	PSHA + spectral matching	Artificial ground motions generated	No soil amplification; different tectonic setting from Bali
Kurniawan et al. (2019). [7]	Lombok, NTB	PSHA vulnerability mapping	Seismic zonation maps produced	No site response or amplification analysis
Hanindya et al. (2023). [17]	General Indonesia	DSHA for liquefaction	Liquefaction potential framework	Deterministic only; no PSHA; no spectral matching
Pawirodikromo et al. (2025). [18]	Indonesia (multi-city)	PSHA + inelastic structural response	3-D building response from PSHA motion	Not site-specific to Bali; no soil amplification at the airport
Present study	Bali Airport (site-specific)	PSHA + soil amplification + spectral matching	Bedrock PGA = 0.308 g; surface PGA = 0.800 g	First integrated study for this critical facility

METHODOLOGY

The study site is I Gusti Ngurah Rai International Airport, located in Tuban Village, Badung Regency, Bali, Indonesia (coordinates: 8.748°S, 115.167°E). The airport occupies reclaimed coastal land along the Jimbaran Bay shoreline and is underlain by Quaternary alluvial and beach sediments, resting on volcanic bedrock of the Buyan–Bratan Formation. The geological and geotechnical setting, characterized by a shallow water table and soft-to-medium alluvial soils, predisposes the site to strong ground-motion amplification and liquefaction.

Figure 1. Location of the source research building, Google Maps

The PSHA was performed using EZ-FRISK (Risk Engineering Inc.), a widely validated commercial software platform for probabilistic hazard analysis [19]. The following key assumptions and parameter choices were made:

- Earthquake occurrence follows a Poisson process; events are temporally independent with a constant average rate.
- The magnitude range for integration is Mmin = 4.0 to Mmax = 9.0; events below Mmin are assumed to cause negligible structural damage.
- Three seismic source types were modeled: (i) Java–Bali interface megathrust (depth 15–50 km), (ii) intraslab events (depth 50–200 km), and (iii) shallow crustal sources (depth < 15 km). Source geometry and slip rates were obtained from PuSGeN 2017 [4].
- Seismicity parameters (a-value and b-value) were computed by maximum-likelihood regression of the declustered USGS catalog (1900–2025, radius 500 km). The b-value was determined to be 0.92 ± 0.05 for the Bali region.
- The GMPE of Atkinson and Boore (2003) [13] was selected for subduction sources due to its extensive validation for similar tectonic environments (Cascadia, Japan, Southeast Asia). A logic tree with two

additional GMPEs, BC Hydro (Abrahamson et al. 2016 [14]) and Zhao et al. (2006) [15], was included to capture epistemic uncertainty, with weights 0.40, 0.35, and 0.25, respectively.

- Aleatory variability (sigma) in ground motion is propagated by integrating over ±3 standard deviations of the GMPE prediction.
- The target hazard level is 2% probability of exceedance in 50 years, corresponding to a return period of 2,475 years, consistent with SNI 1726:2019 [5].

One-dimensional non-linear equivalent-linear site response analysis was performed using DEEPSOIL V7 [16]. Soil profiles were constructed from N-SPT borehole logs at the airport site. Shear-wave velocity (Vs) was estimated from N-SPT blow counts using the Imai and Tonouchi (1982) [20] correlation. The modulus reduction (G/Gmax) and damping ratio curves of Darendeli (2001) [21] were applied for cohesive soils; Seed and Idriss (1970) [22] curves were used for cohesionless layers. Input bedrock motions were the seven spectrally matched accelerograms from the PEER NGA-West2 database, selected to represent the deaggregation-derived dominant scenario (Mw 5.95, R = 23.86 km). The mean surface response spectrum from the seven records was adopted as the design surface spectrum.

Ground motions were selected from the PEER NGA-West2 database [23] based on compatibility with the target magnitude, distance, and site class. Seven records were matched to the target UHS using SeismoMatch (Seismosoft), which iteratively modifies the wavelet content of each record to minimize spectral mismatch while minimizing time-domain alterations. The matching was performed across the period range 0.01–4.0 s, consistent with the range of structural natural periods relevant to airport building types.

Liquefaction potential was evaluated using the simplified procedure of Youd et al. (2001) [24] as updated by Idriss and Boulanger (2008) [25]. The Cyclic Stress Ratio (CSR) was computed from the surface PGA (0.800 g) and total/effective overburden stresses. The Cyclic Resistance Ratio (CRR) was derived from N-SPT values corrected for overburden, energy, borehole diameter, and rod length (N1,60). The Factor of Safety against liquefaction (FS_liq = CRR/CSR) was computed layer by layer. Layers with FS_liq < 1.0 were identified as liquefiable.

The complete research procedure is illustrated in Figure 1, encompassing data collection, PSHA computation, deaggregation, ground motion selection and matching, site response propagation, and liquefaction assessment.

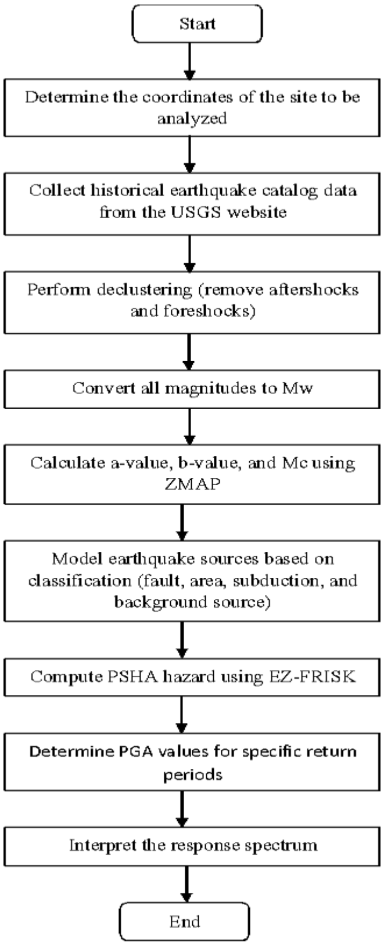

Figure 2*. Research methodology flowchart*

RESULT AND DISCUSSION

PSHA Results: Uniform Hazard Spectrum

Figure 3 presents the Uniform Hazard Spectrum (UHS) at bedrock for the 2%/50-year hazard level. Table 3 lists the spectral acceleration values Sa(T) and their 2/3 design values across the period range 0.00–4.00 s. The 2/3 factor is applied in accordance with SNI 1726:2019 Section 6.2, which reduces the maximum considered earthquake (MCE) spectrum to the design basis earthquake (DBE) level**.**

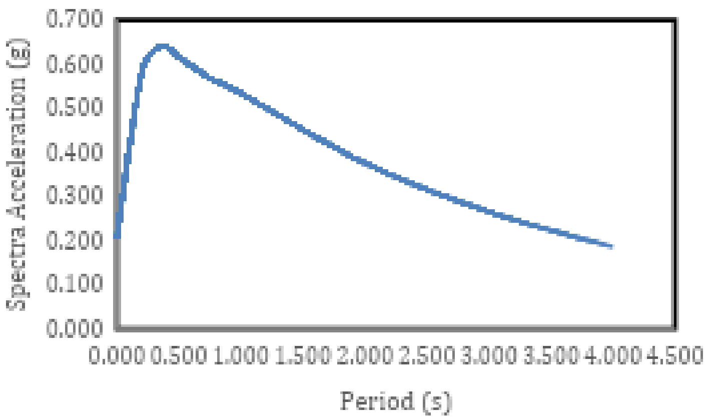

Figure 3. *Uniform Hazard Spectrum (UHS) at bedrock 2% probability of exceedance in 50 years (return period = 2,475 years). Horizontal axis: period T (s); vertical axis: spectral acceleration Sa (g).*

Tabel. Table PSHA results: bedrock spectral acceleration at 2%/50-year hazard level

Period **(s)**	***Spectral Accelation*** **(g)**	**2/3** ***Spectral Acceleration*** **(g)**
0,000	0,308	0,206
0,050	0,464	0,309
0,100	0,615	0,410
0,200	0,871	0,581
0,300	0,946	0,630
0,400	0,959	0,639
0,500	0,925	0,617
0,750	0,854	0,569
1,000	0,802	0,534
2,000	0,563	0,376
3,000	0,398	0,265
4,000	0,279	0,186

The bedrock PGA of 0.308 g is consistent with the PuSGeN 2017 national hazard map value for the Badung–Denpasar corridor (approximately 0.30–0.35 g), providing cross-validation of the PSHA results. Peak spectral demand occurs near T = 0.3–0.4 s, reflecting dominance of moderate-magnitude, near-field subduction events in the hazard. This period range corresponds to the natural period of low-to-mid-rise rigid reinforced concrete structures typical of airport terminal buildings, implying high structural demand on these facility types.

Hazard Deaggregation

Figure 3 shows the deaggregation of PGA hazard (T = 0 s) and short-period spectral hazard (T = 0.2 s) at the 2%/50-year level. Deaggregation reveals the relative contribution of each magnitude–distance combination to the total hazard exceedance probability.

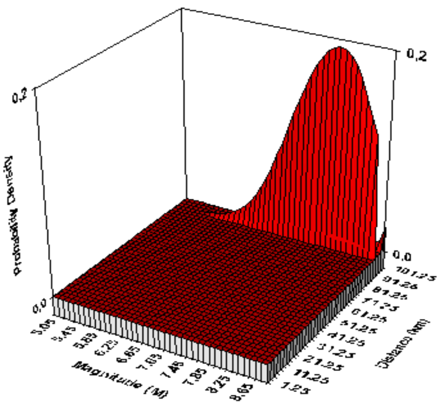

Figure 4. *Hazard deaggregation at (a) PGA period T = 0 s and (b) T = 0.2 s 2% probability of exceedance in 50 years. Bar heights indicate fractional contribution to total hazard; horizontal axes show moment magnitude Mw and source-to-site distance R (km)*

The dominant hazard scenario at both periods is characterized by a mean magnitude of Mw 5.95 and a mean distance of 23.86 km, contributed primarily by shallow crustal faults in the Badung–Tabanan fault system. Subduction interface sources (Mw 7.5–8.5, R > 100 km) contribute approximately 30% of the hazard at longer periods (T = 1.0 s) despite their greater distance, due to their large magnitudes. This dual-source hazard composition, with near-field shallow sources dominating short-period hazard and far-field megathrust sources controlling long-period demand, has important implications for ground-motion selection. Both source types should be represented in structural analysis.

The actual time history that is closest to M and R, which is the dominant result of *Probabilistic Seismic Hazard Analysis*, is *the time history record.* Because it is used for structural analysis, the selection of the actual time history must reflect the content of high-, medium-, and low-frequency components, as stated by previous researchers.

Ground Motion Selection and Spectral Matching

Seven accelerogram records from the PEER NGA-West2 database were selected consistent with the dominant deaggregation scenario (Mw ≈ 5.9–6.1, R = 15–35 km, site class C/D). Figure 4 shows the target UHS alongside the pre- and post-matching individual response spectra and their mean. After matching with SeismoMatch, the mean spectrum is within ±10% of the target across the 0.01–4.0 s period range, satisfying the tolerance specified in SNI 1726:2019 and ASCE 7-22

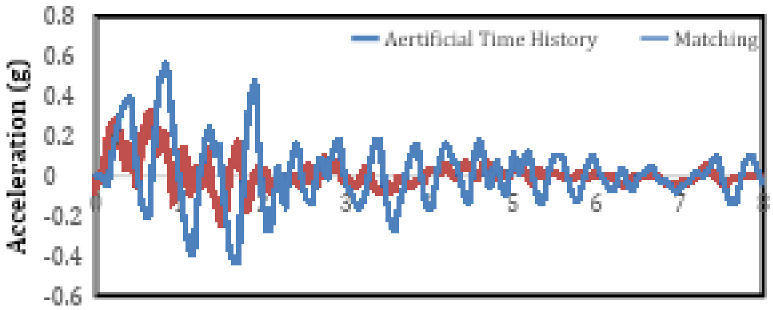

Figure 5. *Spectral matching results: (a) pre-matching individual spectra and mean vs. target UHS; (b) post-matching spectra confirming mean within ±10% tolerance. Vertical axis: spectral acceleration Sa (g); horizontal axis: period T (s)*

Soil Amplification and Surface Ground Motion

Figure 6 shows the borehole log and derived Vs profile used as input for the DEEPSOIL site response analysis. The uppermost 20 m consists of loose to medium-dense alluvial sand and silty clay (N-SPT = 5–18 blows/30 cm; Vs = 120–220 m/s), underlain by medium-dense to dense volcanic sand (N-SPT = 25–50; Vs = 300–450 m/s). Computed Vs30 = 218 m/s classifies the site as Site Class D (soft soil) per SNI 1726:2019, confirming that default code amplification factors may underestimate actual ground motion at this site.

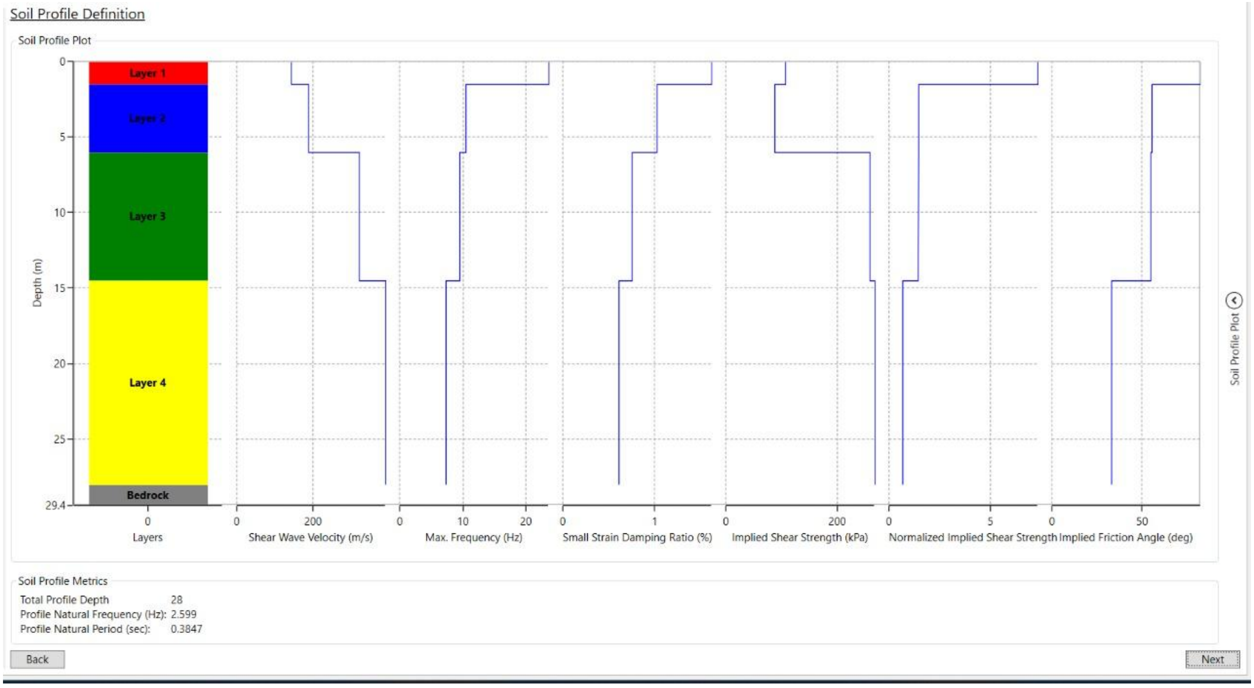

Figure 6. *Borehole log and shear-wave velocity (Vs) profile at Bali Airport. Left panel: soil classification and N-SPT values; right panel: Vs (m/s) versus depth (m) derived from Imai–Tonouchi correlation.*

Figure 7 presents the mean surface response spectrum from DEEPSOIL propagation compared to the bedrock input spectrum. The amplification factor (surface Sa / bedrock Sa) peaks at approximately 2.6 near T = 0.5–0.8 s, corresponding to the natural frequency of the soft soil column (fundamental period = 0.6 s). This resonance effect, in which the soil column's natural period coincides with the input motion frequency content, is the primary physical mechanism driving amplification at this site. The surface PGA reaches 0.800 g compared to the bedrock value of 0.308 g.

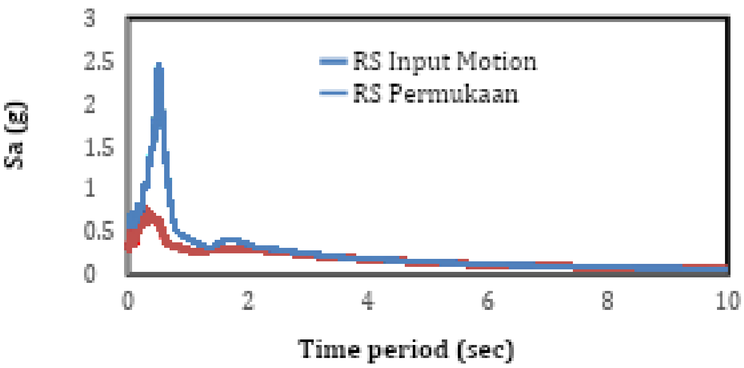

Figure 7. *Comparison of mean surface response spectrum (after DEEPSOIL propagation) with bedrock input spectrum 2%/50-year hazard level. Shading shows ±1 standard deviation of the seven-record ensemble—vertical axis: Sa (g); horizontal axis: T (s).*

This level of amplification (factor ≈ 2.6) substantially exceeds the SNI 1726:2019 default Site Class D short-period amplification factor (Fa ≈ 1.7 for high seismic regions), indicating that the site-specific analysis provides a significantly more accurate and conservative estimate of surface hazard than code defaults. Engineers designing airport structures using only national maps without site-specific analysis would underestimate the design demand by approximately 53%.

Hysteretic Soil Behavior

Figure 8 shows the hysteretic shear stress–shear strain loops for the critical soil layer (depth ≈ 5–10 m) computed by DEEPSOIL. The elliptical loops demonstrate non-linear inelastic soil behavior under cyclic seismic loading: energy dissipation (damping) is represented by the area enclosed within each loop. The effective damping ratio for this layer reached approximately 18–22% at peak strain, substantially higher than the small-strain damping (≈ 5%), confirming significant non-linearity in the soft upper stratum. This non-linear response validates the choice of equivalent-linear analysis and highlights the inadequacy of the linear elastic assumption for this site.

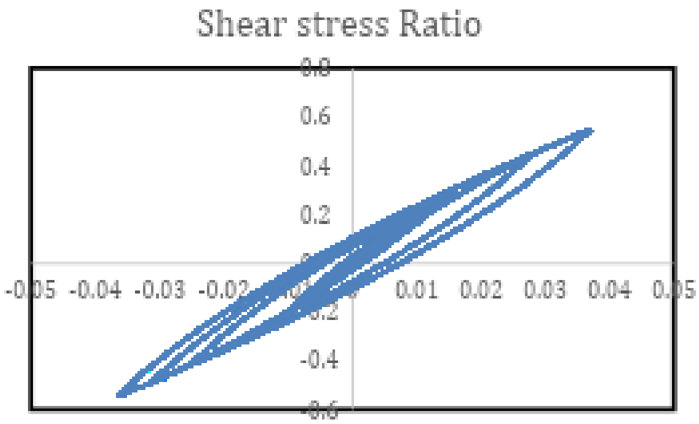

Figure 8. *Hysteretic shear stress–shear strain loops for the critical soil layer (depth 5–10 m) computed by DEEPSOIL V7. The area enclosed by each loop represents energy dissipated per cycle; wider loops indicate higher effective damping. Vertical axis: shear stress ratio τ/σ'v; horizontal axis: shear strain γ (%).*

Liquefaction Potential

Based on the amplified surface PGA of 0.800 g, the CSR was computed for each soil layer. Layers with N1, 60 < 15 blows/30 cm concentrated in the upper 8 m of the profile exhibit FS_liq < 1.0, indicating high liquefaction susceptibility. The critical layer (depth 3–6 m, N1,60 ≈ 8) yields FS_liq ≈ 0.55, well below the threshold of 1.0. These results confirm significant liquefaction risk at the site under the design-level earthquake, consistent with the findings of Artati et al. (2023) [17] and Ibrohim Burhan et al. (2025) [26] for similar coastal Lombok profiles.

Comparison with Previous Studies

The bedrock PGA of 0.308 g derived in this study is consistent with the PuSGeN 2017 national map value (0.30–0.35 g) and with Asrurifak et al. (2010) [1], who reported PGA values of approximately 0.25–0.35 g across Bali for a 2,500-year return period. The amplification factor of 2.6 observed at this site is higher than typical values reported for Lombok (1.8–2.0; Kurniawan et al. 2019 [7]) and Semarang (1.5–2.2; Makrup and Muntafi 2016 [6]), reflecting the particularly soft alluvial sediments at the coastal airport site. This comparison underscores the site-specific nature of amplification and reinforces the need for site-specific studies rather than relying on national-level maps for critical infrastructure.

CONCLUSION

1. Site-specific PSHA at I Gusti Ngurah Rai International Airport yields a bedrock PGA of 0.308 g (design PGA = 0.206 g) for a 2% probability of exceedance in 50 years. These values are consistent with the national

PuSGeN 2017 hazard map, validating the PSHA methodology. The Uniform Hazard Spectrum peaks at T = 0.3–0.4 s, indicating a high spectral demand on low- to mid-rise rigid structures typical of airport facilities.

2. Hazard deaggregation identifies a dominant scenario earthquake of Mw 5.95 at a mean distance of 23.86 km, primarily contributed by shallow crustal fault sources. Far-field megathrust events (Mw 7.5–8.5) become significant contributors to long-period hazard (T > 1.0 s). Both source types should be included in the selection of ground motion for the structural analysis of airport buildings.

3. Spectral matching of seven PEER NGA-West2 records to the target UHS produced mean spectra within ±10% of the target across 0.01–4.0 s, satisfying SNI 1726:2019 and ASCE 7-22 tolerances. These matched motions provide reliable input time histories for dynamic structural analysis of airport infrastructure.

4. One-dimensional non-linear site response analysis (DEEPSOIL V7) reveals substantial soil amplification driven by resonance between the soft alluvial column (Vs30 = 218 m/s; fundamental period ≈ 0.6 s) and the bedrock input motion. Surface PGA reaches 0.800 g, with an amplification factor of approximately 2.6, significantly exceeding the default SNI 1726:2019 Site Class D amplification factor (Fa ≈ 1.7). Designers relying solely on code defaults without site-specific analysis would underestimate surface demand by ≈ 53%.

5. Liquefaction assessment based on the amplified surface PGA indicates high liquefaction susceptibility in the upper 8 m of the profile (FS_liq ≈ 0.55–0.90 in critical layers). Ground improvement or deep foundation solutions are strongly recommended for any new airport structures or runway pavement rehabilitation at this site.

Study Limitations

The following limitations should be considered when applying these results: (i) the PSHA relies on a single borehole log; spatial variability of the soil profile across the large airport footprint is not captured and should be addressed in future studies with a multi-borehole investigation; (ii) only one GMPE family (Atkinson and Boore 2003 with logic-tree extensions) was applied to subduction sources future studies should employ a broader GMPE logic tree; (iii) liquefaction assessment used the simplified N-SPT procedure; laboratory cyclic triaxial tests on undisturbed samples would provide higher accuracy; (iv) three-dimensional basin and topographic effects were not considered.

Recommendations for Future Research

Future work should conduct multi-point borehole campaigns to map spatial variability of Vs and N-SPT across the airport; apply advanced non-linear site response analysis (fully non-linear DEEPSOIL mode) to capture large-strain behaviour at 0.800 g PGA better, extend the PSHA logic tree to include 3–4 additional subduction GMPEs (e.g., Abrahamson et al. 2016 BC Hydro; Zhao et al., 2006); perform 2-D or 3-D basin response analysis to capture edge effects at the coastal boundary; carry out field CPT and laboratory cyclic triaxial tests for refined liquefaction assessment; and integrate the hazard results into a performance-based earthquake engineering (PBEE) framework to quantify expected losses and guide airport business-continuity planning.

Acknowledgment

This study was supported by the Kemitraan Negara Berkembang (KNB) Scholarship, provided by the Ministry of Higher Education, Sciences, and Technology of the Republic of Indonesia, on behalf of the Government of the Republic of Indonesia. The views expressed in this publication are solely those of the author, and the Ministry of Higher Education, Sciences, and Technology of the Republic of Indonesia cannot be held liable for any use that may be made of the information contained herein.

The author extends sincere gratitude to all parties who contributed to the success of this research and publication. Special thanks are given to the lecturers for their invaluable guidance and extraordinary materials, which played a crucial role in completing this work. Additionally, heartfelt appreciation is extended to the Faculty of Civil Engineering and Planning at the Islamic University of Indonesia for providing an excellent platform for academic development, as well as to the Civil Engineering Study Program for serving as the foundation of the author's academic journey.

REFERENCES

[1] Asrurifak, M., Irsyam, M., Budiono, B., Triyoso, W., & Hendriyawan. (2010). Development of Spectral Hazard Map for Indonesia with a Return Period of 2500 Years using Probabilistic Method. Civil Engineering Dimension, 12(1), 52–62. https://doi.org/10.9744/ced.12.1.52-62

[2] Koulali, A., Tregoning, P., McClusky, S., Stanaway, R., Wallace, L., & Lister, G. (2016). New insights into the present-day kinematics of the central and western Papua New Guinea from GPS. Geophysical Journal International, 206(2), 888–897. https://doi.org/10.1093/gji/ggw171

[3] Angkasa Pura I. (2023). Annual Report 2022: Traffic Statistics. PT Angkasa Pura I (Persero), Jakarta.

[4] PuSGeN. (2017). Peta Sumber dan Bahaya Gempa Indonesia Tahun 2017. Badan Penelitian dan Pengembangan Kementrian Pekerjaan Umum dan Perumahan Rakyat. ISBN 978-602-5489-01-3.

[5] BSN. (2019). SNI 1726:2019 – Tata Cara Perencanaan Ketahanan Gempa untuk Struktur Bangunan Gedung dan Non-Gedung. Badan Standardisasi Nasional, Jakarta.

[6] Makrup, L. L., & Muntafi, Y. (2016). Artificial Ground Motion for the Cities of Semarang and Solo Indonesia Generated Based on Probabilistic Seismic Hazard Analysis and Spectral Matching. EJGE, 21(21), 6587–6602.

[7] Kurniawan, A., Basuki, A., & Permana, D. (2019). Pemetaan kerentanan bencana gempa bumi menggunakan metode Probabilistic Seismic Hazard Analysis (PSHA) Lombok, Nusa Tenggara Barat. Jurnal Teknik Sipil, 8(2), 115–126.

[8] Anugrayanti, A., Arsyad, M., & Tiwow, V. A. (2021). Analysis of Susceptible Disaster Region Based on The Peak Ground Acceleration and Earthquake Intensity in Mamasa 2018. Journal of Physics: Conference Series, 1816(1), 012014. https://doi.org/10.1088/1742-6596/1816/1/012014

[9] Cornell, C. A. (1968). Engineering seismic risk analysis. Bulletin of the Seismological Society of America, 58(5), 1583–1606. https://doi.org/10.1785/BSSA0580051583

[10] McGuire, R. K. (1976). FORTRAN Computer Program for Seismic Risk Analysis (Open-File Report 76-67). U.S. Geological Survey.

[11] McGuire, R. K. (2004). Seismic Hazard and Risk Analysis. Earthquake Engineering Research Institute Monograph MNO-10, Oakland, CA.

[12] Gutenberg, B., & Richter, C. F. (1944). Frequency of earthquakes in California. Bulletin of the Seismological Society of America, 34(4), 185–188.

[13] Atkinson, G. M., & Boore, D. M. (2003). Empirical Ground-Motion Relations for Subduction Zone Earthquakes and Their Application to Cascadia and Other Regions. Bulletin of the Seismological Society of America, 93(4), 1703–1729. https://doi.org/10.1785/0120020156

[14] Abrahamson, N. A., Gregor, N., & Addo, K. (2016). BC Hydro Ground Motion Prediction Equations for Subduction Earthquakes. Earthquake Spectra, 32(1), 23–44. https://doi.org/10.1193/051712EQS188MR

[15] Zhao, J. X., Zhang, J., Asano, A., Ohno, Y., Oouchi, T., Takahashi, T., Ogawa, H., Irikura, K., Thio, H. K., Somerville, P. G., Fukushima, Y., & Fukushima, Y. (2006). Attenuation Relations of Strong Ground Motion in Japan Using Site Classification Based on Predominant Period. Bulletin of the Seismological Society of America, 96(3), 898–913. https://doi.org/10.1785/0120050122

[16] Hashash, Y. M. A., Musgrove, M. I., Harmon, J. A., Ilhan, O., Xing, G., Numanoglu, O., Groholski, D. R., Phillips, C. A., & Park, D. (2020). DEEPSOIL 7.0, User Manual. University of Illinois at Urbana-Champaign, Urbana, IL.

[17] Hanindya, K. A., Makrup, L., Widodo, & Rahardjo, P. (2023). Deterministic Seismic Hazard Analysis to Determine Liquefaction Potential Due to Earthquake. Civil Engineering Journal (Iran), 9(5), 1203–1216. https://doi.org/10.28991/CEJ-2023-09-05-012

[18] Pawirodikromo, W., & Makrup, L. (2025). Respons Inelastik Struktur Bangunan Gedung Bertingkat 3-Dimensi Akibat Gerakan Tanah Berdasarkan Probabilistic Seismic Hazard Analysis. Jurnal Teknik Sipil (JTSP), 27(1), 1–16.

[19] Risk Engineering Inc. (2017). EZ-FRISK 8.0: Software for Earthquake Ground Motion Estimation. Boulder, Colorado.

[20] Imai, T., & Tonouchi, K. (1982). Correlation of N-value with S-wave velocity and shear modulus. Proceedings of the 2nd European Symposium on Penetration Testing, Amsterdam, 57–72.

[21] Darendeli, M. B. (2001). Development of a New Family of Normalized Modulus Reduction and Material Damping Curves. PhD Dissertation, University of Texas at Austin.

[22] Seed, H. B., & Idriss, I. M. (1970). Soil Moduli and Damping Factors for Dynamic Response Analysis (Report No. EERC 70-10). Earthquake Engineering Research Center, University of California, Berkeley.

[23] PEER. (2024). PEER NGA-West2 Ground Motion Database. Pacific Earthquake Engineering Research Center, University of California, Berkeley. https://ngawest2.berkeley.edu

[24] Youd, T. L., Idriss, I. M., Andrus, R. D., Arango, I., Castro, G., Christian, J. T., Dobry, R., Finn, W. D. L., Harder, L. F., Hynes, M. E., Ishihara, K., Koester, J. P., Liao, S. S. C., Marcuson, W. F., Martin, G. R., Mitchell, J. K., Moriwaki, Y., Power, M. S., Robertson, P. K., Seed, R. B., & Stokoe, K. H. (2001). Liquefaction resistance of soils: Summary report from the 1996 NCEER and 1998 NCEER/NSF Workshops on Evaluation of Liquefaction Resistance of Soils. Journal of Geotechnical and Geoenvironmental Engineering, 127(10), 817–833.

[25] Idriss, I. M., & Boulanger, R. W. (2008). Soil Liquefaction During Earthquakes (Monograph MNO-12). Earthquake Engineering Research Institute, Oakland, CA.

[26] Ibrohim Burhan, L., Kusuma Artati, H., Makrup, L., & Saputra, E. (2025). Liquefaction potential study under Ijo Balit weir in East Lombok, Indonesia. Teknisia, 30(1), 23–32. https://doi.org/10.20885/teknisia.vol30.iss1.art3

[27] Artati, H., Pawirodikromo, W., Rahardjo, P., & Makrup, L. (2023). Effect of Fines Content on Liquefaction Resistance During Steady-State Conditions. International Journal of GEOMATE, 25(109), 18–28. https://doi.org/10.21660/2023.109.3481

[28] Abbas, M., Elbaz, K., Shen, S.-L., & Chen, J. (2021). Earthquake effects on civil engineering structures and perspective mitigation solutions: A review. Arabian Journal of Geosciences, 14, 1350. https://doi.org/10.1007/s12517-021-07664-5

[29] Muh. S. L., Siraj Ramadhan, A., Kusmiran, A., Priadi, R., & Alamsyah, A. (2023). Analisis Kecocokan Nilai PGA Metode Donovan Terhadap Data Accelerograph (Studi Kasus Gempa Bali, 14 Januari 2021). Journal of Online Physics, 8(2), 29–36. https://doi.org/10.22437/jop.v8i2.21884

[30] Stewart, J. P., Luco, N., Hooper, J. D., & Crouse, C. B. (2020). Risk-targeted alternatives to deterministic ground motion caps in U.S. seismic provisions. Earthquake Spectra, 36(2), 904–923. https://doi.org/10.1177/8755293019892010

[31] Sari, I. N., & Prastowo, T. (2022). Analysis of Seismicity and Potential Hazards of Seismic Disasters in the Southern Region of Sumatra Island. Indonesian Physics Innovation, 11(2), 12–19.

[32] Uyanık, O. (2020). Soil liquefaction analysis based on soil and earthquake parameters. Journal of Applied Geophysics, 176, 104004. https://doi.org/10.1016/j.jappgeo.2020.104004

[33] Yuan, J., Wang, Y., Zhan, B., Yuan, X., Wu, X., & Ma, J. (2022). Comprehensive investigation and analysis of liquefaction damage caused by the Ms7.4 Maduo earthquake in 2021 on the Tibetan Plateau, China. Soil Dynamics and Earthquake Engineering, 155, 107191. https://doi.org/10.1016/j.soildyn.2022.107191

[34] Silvia, U. N., & Maimuna, A. K. (2020). Analysis of the Risk Level and Vulnerability of Earthquake Hazards in the City of Surabaya in an Effort to Provide Disaster Mitigation Information. Journal of Meteorology, Climatology and Geophysics, 7(3), 51–57.